Title: Nanocomposite Ag:TiN thin films for dry biopotential electrodes

Author: P. Pedrosa D. Machado C. Lopes E. Alves N.P. Barradas N. Martin F. Macedo C. Fonseca F. Vaz

PII: S0169-4332(13)01465-7
DOI: http://dx.doi.org/doi:10.1016/j.apsusc.2013.07.154
Reference: APSUSC 26128

To appear in: *APSUSC*

Received date: 3-4-2013
Revised date: 30-7-2013
Accepted date: 30-7-2013

Please cite this article as: P. Pedrosa, D. Machado, C. Lopes, E. Alves, N.P. Barradas, N. Martin, F. Macedo, C. Fonseca, F. Vaz, nanocomposite Ag:TiN thin films for dry biopotential electrodes, *Applied Surface Science* (2013), http://dx.doi.org/10.1016/j.apsusc.2013.07.154

NANOCOMPOSITE Ag:TiN THIN FILMS FOR DRY BIOPOTENTIAL ELECTRODES

P. Pedrosa[1,2,3], D. Machado[3], C. Lopes[3], E. Alves[4], N.P. Barradas[5], N. Martin[6], F. Macedo[3], C. Fonseca[1,2], F. Vaz[3*]

[1]SEG-CEMUC – Department of Mechanical Engineering, University of Coimbra, Portugal

[2]Universidade do Porto, Faculdade de Engenharia, Departamento de Engenharia Metalúrgica e de Materiais, Rua Roberto Frias, s/n, 4200-465 Porto, Portugal

[3]Centro de Física, Universidade do Minho, 4710-057 Braga, Portugal

[4]Associação Euratom/IST, Instituto de Plasmas e Fusão Nuclear, Instituto Superior Técnico, Universidade Técnica de Lisboa, Av. Rovisco Pais, 1049-001, Lisboa, Portugal

[5]Campus Tecnológico Nuclear, Instituto Superior Técnico, Universidade Técnica de Lisboa, E.N. 10, 2686-953 Sacavém, Portugal

[6]Institut FEMTO-ST, UMR 6174, Université de Franche-Comté, CNRS, ENSMM, UTBM, 32, Avenue de l'observatoire, 25044 BESANÇON Cedex, France

ABSTRACT

Silver-added titanium nitride (Ag:TiN) thin films were deposited by DC reactive sputtering with Ag contents ranging from 0 to ~50 at.% on silicon and glass substrates, aiming at studying their potential application as bio-electrodes. The coatings were characterized regarding their composition, morphology and structure, and their influence on the variation of the electrical resistivity and thermal properties. The sputtered films' behaviour was consistently divided into three main zones, defined mainly by the amount of Ag incorporated and the correspondent changes in the structural and morphological features, which affected both the electrical and thermal response of the films. With increasing Ag concentration, the coatings evolve from a nitride/compound-like behaviour to a metallic-like one. Resistivity values suffer a strong decrease due to the increase of

*To whom all correspondence should be sent (fvaz@fisica.uminho.pt)

compactness of the coatings and the formation of highly conductive Ag phases, counterbalancing the grain size decrease effects promoted by the hindered growth of the crystalline TiN phases. In good agreement with the electrical resistivity evolution, a similar trend was found in the effusivity values, reflecting a significant degradation of the heat conduction mechanisms in the films as the silver content was increased.

Keywords: TiN; Ag addition; biopotential electrodes; EEG; ECG; dry electrodes; RBS; XRD; electrical resistivity, thermal properties.

1. INTRODUCTION

For the past few decades, modern medicine has relied on high resolution monitoring of biopotentials produced by the human body, such as electroencephalography (EEG, brain activity), electrocardiography (ECG, heart activity) and electromyography (EMG, muscular activity), in order to accurately comprehend several pathologies and physiological conditions of human patients. The conventional biopotential acquisition set-up relies on the use of the well-known silver/silver chloride (Ag/AgCl) wet electrodes [1-3]. These are considered the "gold standard" electrodes, as they are non-polarizable and reveal excellent reliability, displaying low and almost frequency independent skin-contact impedance values, in the order of a few tens of $k\Omega.cm^2$ [2, 3]. However, a preliminary skin preparation and a gel paste application are needed before the exam, in order to lower the skin/electrode impedance. This preparation is time consuming, uncomfortable to the patient and requires trained staff. Furthermore, some patients have developed severe allergic reactions to the common used gel pastes [3] and the risk of short-circuiting adjacent electrodes due to gel running can be, in some cases, relatively high. Susceptibility to motion artifacts and inability to record biopotentials in long-term clinical monitoring (ambulatory) have also been reported [2, 3].

In order to avoid these and other related drawbacks of the conventional Ag/AgCl electrodes, a new class of devices is being investigated in the group, for which no previous skin preparation or

gel application is needed, the so-called “dry” electrodes. In these electrodes, the sensors are based on inert-like materials, either metallic-like or even of insulating type [3, 4]. In a previous work [5], the authors investigated a type of dry electrode sensor, based on a titanium nitride (TiN) thin film, deposited on a titanium substrate. Despite the promising results, these electrodes, as well as other similar dry electrodes [6, 7], are quite rigid, which can give rise to an incorrect and uncomfortable skin contact, due to the inherent irregular nature of the human skin. In addition, taking into account the particular case of an EEG recording set-up, which may involve the use of 128 or even 256 electrodes in a single exam, the use of lighter, cheaper and more comfortable electrodes would translate in numerous advantages in comparison with the standard Ag/AgCl ones.

The use of polymer-based electrodes, namely the flexible ones, would fill in this gap, as they would surpass most of the problems stated above. Recently, several authors have focused on the development of flexible dry electrodes [8-11]. However, there are still some drawbacks inherent to these electrodes, namely higher impedances at low frequencies and they are also more susceptible to movement artefacts than the standard wet Ag/AgCl ones [1, 3, 7]. In fact, the absence of conductive gel has a key influence on the exhibited higher impedances and movement artefacts susceptibility, once the gel can act as a “pillow”, increasing and stabilizing the contact area (higher and well-defined contact areas are of paramount importance to achieve low contact impedances [10]). This is particularly important in ambulatory applications, where the patient must be able to move freely. Consequently, and in opposition to most common approaches (where authors rely on rigid metal plates or composite materials – foams/conductive polymers), the present work aims at studying Ag:TiN nanocomposite thin films, and assessing their suitability to be sputtered on flexible polymers (to better adapt to the skin and mitigate some of the drawbacks stated above), so that they could be used as flexible dry biopotential electrodes.

Reactive DC magnetron sputtering is commonly accepted as one of the most versatile and less expensive techniques, being widely assumed as able to produce fairly high deposition rates and compact coatings, when compared to other techniques. TiN is an electrically conductive coating,

with an excellent chemical stability in most media and outstanding mechanical properties, which led to a very broad range of applications, including those in the biomedical area [12, 13]. Furthermore, TiN is biocompatible, but it is also a relatively hard and high Young's modulus material, thus unable to withstand large deformations (in fact, most metallic films tolerate less than 10% of deformation [14-21]). It gives rise to mechanical failure of the coatings, which, in turn, is highly undesirable when the objective is to produce flexible electrodes that are supposed to adapt to the human skin. The inclusion of silver, due to its intrinsic characteristics, particularly the low Young's modulus and high conductivity [22], within the TiN films may offer the possibility to tailor the Young's modulus of the coating [23], opening a wide range of possible applications, namely those related to the coating of flexible devices such as polymers. Furthermore, silver addition may also allow the tailoring of the materials' electrical conductivity [24], which may be of crucial importance in any electrode-based application. Finally, silver is inherently antimicrobial [25-27], particularly in its nanocrystalline form [28, 29] and has the ability to stabilize the electrochemical potential [30], which is of major importance in any application that may involve electrophysiological signal monitoring.

Starting with both TiN and silver characteristics, the main goal of the present work is to provide a detailed study on the influence of silver addition to titanium nitride, optimizing the deposition conditions in order to obtain conductive and mechanically suitable films to coat flexible polymeric-type substrates and with enough bactericide character that may give the as-prepared thin films a set of characteristics to be used in biopotential electrodes.

2. EXPERIMENTAL DETAILS

Ag:TiN films were deposited on glass and (100) silicon substrates by reactive DC magnetron sputtering, in a laboratory-sized deposition system. All substrates were sonicated and cleaned with ethanol 96% (vol.) just before each deposition. The films were prepared with the substrate holder positioned at 70 mm from the Ti/Ag composite target. A DC current density of 100 $A.m^{-2}$ was

applied to the composite target, composed of titanium (99.96 at.% purity / 200×100×6 mm^3) and silver pellets (0.8×0.8 cm^2 / 1 mm thick pellets glued on the surface of the target) distributed symmetrically along the erosion area. The total surface area of the silver pallets varied between 0.75 to 8.3 cm^2. A gas atmosphere composed of argon + nitrogen was used. The argon flow was kept constant at 60 sccm for all depositions, as well as the nitrogen flow rate, which was set at 5 sccm (corresponding to a partial pressure of 3.4×10^{-2} Pa). The working pressure was approximately constant during the depositions, varying only slightly between 0.35 and 0.38 Pa. No bias voltage was used, and the deposition temperature was maintained approximately constant at 100 ºC during the films' growth. A thermocouple was placed close to the surface of the "substrate holder" on the plasma side (not in direct contact, since all depositions were done in rotation mode), and the temperature was monitored during the entire films' deposition time. A delay time of five minutes was used before positioning the surface of the samples in front of the Ti/Ag target in order to avoid films' contamination resulting from previous depositions (which may have resulted in some target poisoning), and also to assure a practically constant deposition temperature during the films' growth.

The atomic composition of the as-deposited samples was measured by Rutherford Backscattering Spectroscopy (RBS) using (1.4, 2.3) MeV and (1.4, 2) MeV for the proton and ^4He beams, respectively. Three detectors were used. One located at a scattering angle of 140º and two pin-diode detectors located symmetrical to each other, both at 165º. Measurements were made for two sample tilt angles, 0º and 30º. Composition profiles for the as-deposited samples were determined using the software NDF [31]. For the ^{14}N, ^{16}O and ^{28}Si data, the cross-sections given by Gurbich were used [32]. The area analysed was about 0.5×0.5 mm^2. The uncertainty in the N concentrations is around 5 at.%. The structure and phase distribution of the coatings were assessed by X-ray diffraction (XRD), using a Bruker AXS Discover D8 diffractometer, operating with Cu K_α radiation and in a Bragg-Brentano configuration. The XRD patterns were deconvoluted and fitted with a Voigt function to determine the structural characteristics of the films, such as the peak

position (2θ), the full width at half maximum (FWHM) and the crystallite size. Morphological features of the samples were probed by scanning electron microscopy (SEM), carried out in a FEI Quanta 400FEG ESEM microscope operating at 15 keV. The resistivity measurements were done using the four-probe van der Pauw method [33]. The thermal characteristics of the coatings were accessed by IR radiometry. The measurement system used is externally controlled by software and consists basically in three main parts: excitation, detection and amplification. The amplification is controlled by a pre-amplifier and a two-phase lock-in amplifier (SR 830 DSP). The amplitude and phase lag relative to the modulated excitation, as a function of the heating modulation frequency, giving information on the thermal wave's properties, are recorded by the lock-in and stored in the main computer. Further details on the technique can be found elsewhere [34].

3. RESULTS AND DISCUSSION

3.1. Discharge characteristics: target potential and deposition rate

In order to study the kinetics and the deposition-related features, the evolution of the target potential during the films' growth, as well as the final growth rates were firstly characterized. Fig. 1 shows the evolution of these two characteristics as a function of the area of the Ag pellets placed on the target. It is worth noting that the amount of silver in the target (illustrated by the increasing area/number of the pellets placed in the target erosion zone) results in a three-fold variation type, which will be further noted as films prepared within zones I, II and III. Within zone I, the prepared thin films can be described as within a TiN-like zone, where both target potential and deposition rates are somewhat similar to the single TiN sputtering conditions due to the small area of Ag exposed (i.e. below 1 cm^2). However, a small change in the behaviour of the studied parameters can be seen with further small additions of Ag. Within zone II, which can be indexed to the incorporation of intermediate amounts of Ag in the target erosion zone, from 1 to 5 cm^2, a small increase of discharge voltage is observed, while growth rate values remain somewhat constant. However, the exhibited values are not very different from the values within zone I. As for zone III,

where larger fractions of Ag are available for sputtering (> 5 cm^2), the increasing of the studied parameters already perceivable in zone II becomes significant. Thus, it is possible to state that both deposition rate and target potential exhibit an overall increasing tendency with increasing areas of Ag exposed in the Ti target. This expected behaviour was explained by Depla et al. [35-37], where the authors studied the effect of several parameters in the ion induced secondary electron emission coefficient (ISEE). One of the referred parameters is the target material dependency of the discharge voltage. At constant current and pressure – corresponding to the conditions used in this work for the preparation of the Ag:TiN coatings – the average ISEE coefficients of the used target materials (Ti and Ag) are rather close, 0.114 and 0.110, respectively. However, based on the Thornton relation [38], it is known that the discharge voltage is inversely proportional to the ISEE coefficient of the target material. Furthermore, one must take into account some poisoning of the Ti fraction of the target during the sputtering process, leading to the formation of nitrides at its surface with a lower ISEE coefficient (0.049 for TiN) [39-42]. This means that the ISEE coefficient of the poisoned fraction of the target will be lower than those stated above for the metallic mode condition (as a result of the TiN poisoning of the Ti fraction of the composite target), while the Ag ISEE coefficient should remain constant, since the formation of AgN is highly improbable thermodynamically, due to the fact that the sputtering of Ag in the presence of nitrogen has an extremely low reactivity [43]. Since the Ag area in the Ti/Ag target is being continuously increased, the Ti poisoning effect is supposed to be gradually reduced, thus a decrease of the target potential values is expected, due to the explained inverse proportionality. However, the opposite behaviour is observed: a slight ~50 V increase of the target potential values is perceivable from ~360 V (low Ag fraction) to ~410 V (high Ag fraction). This effect can probably be ascribed to a gradual covering of the Ti poisoned fraction with Ag, due to strong differences between their sputtering yield values [37], hence altering the discharge characteristics. To note that late zone II and zone III coatings were sputtered with Ag pellets glued (with silver paint) to the target's erosion track, which may also

alter the target and plasma properties, namely its impedance, giving rise to higher potentials as more Ag pellets are placed.

Since the amount of material that is deposited on the substrate per unit of time is correlated with the amount of atoms sputtered from the target, the explanations given above can also, in part, justify the evolution of the sputtering rate, as the decrease of the poisoned Ti fraction of the compound Ti/Ag target should increase the sputtering rate. In fact, zone I and zone II coatings exhibit rather low deposition rates, indicating that the compound target conditions predominate, while the zone III ones were obtained with higher deposition rates. This must be due to the fact that the Ag fraction in the Ti/Ag target is high enough to somewhat deplete the poisoning effect of the Ti fraction responsible for the low sputtering rates present in both zones I and II.

In a review paper, Smentkowski [44] explained the theoretical concept of sputtering yield, which can be defined by:

$$Y = \Lambda \, Fd_{(Eo)} \quad (1)$$

where Λ contains all of the material properties such as the surface binding energies (which is lower for Ag 3d than that of Ti 2p [45]) and $Fd_{(Eo)}$ is the density of energy deposited at the surface, depending on the mass, energy, and direction of the incident ion, as well as the composition of the target. As the other deposition parameters were maintained constant during all depositions in the present work, the composition of the target is of paramount importance to explain the influence of the sputtering yield on the evolution of the sputtering rate. Furthermore, and since the surface binding energy of Ag is lower than that of Ti, the sputtering yield follows the inverse relation. Smentkowski data [44] show experimental and calculated Ag sputtering yields almost seven times higher than Ti (~2.5 and ~0.35, respectively for 400 eV Xe ion bombardment). Consequently, with increasing Ag fraction in the Ti/Ag target, an increase of the deposition rate is expected, once the TiN thin layer poisoning effect is depleted and Ag sputtering yield (and binding energy) is higher than that of Ti.

3.2. Composition of the as-deposited samples

The evolution of the deposition rate and target potential, as well as the increase of Ag fraction in the target will also be correlated with changes in the composition of the films. Fig. 2a) shows the Ag chemical composition (at.%) results and the Ag/(Ti+N) ratio of the Ag:TiN coatings obtained from RBS spectra analysis, while Fig. 2b) exhibits the ternary phase diagram of the deposited samples. Once again, the same three distinct zones are perceivable. Due to the very low area of Ag available for sputtering, the Ag content in the films from zone I is also very low. Besides the TiN reference coating (N/Ti ratio ~1), only one more sample (~0.1 at.% Ag) is ascribed to this zone. Both deposition rate and target potential are quite low in this zone (which can also explain the low incorporation of Ag), but also in zone II. However, in this zone, one can observe an almost linear increase of Ag incorporation in the coatings with the increase of Ag exposed area. This could mean that the much higher Ag sputtering yield is taking control over the composition evolution process, as the Ag content in this area increases steadily from ~4 at.% to ~35 at.% with the increasing area of Ag (number of Ag pellets) available for sputtering in the target. As for zone III films, the increase of Ag content is smoother than in Zone II, with Ag concentrations ranging from ~35 at.% to ~45 at.%, indicating that probably some kind of Ag saturation is being attained. Despite no films with further Ag concentration were produced, taking into account the results exhibited by the last two samples, one can say that the Ag concentration is practically constant (~45 at.%). Regarding the Ag/(Ti+N) ratio, it directly correlates with the Ag content evolution, exhibiting an almost identical linear increase vs. Ag fraction in the target. It is worth to note that the last two samples from zone III, despite having similar Ag contents, do not present the same Ag/(Ti+N) ratio, indicating that the N/Ti ratio (initially ~1) is not constant. As the Ag fraction in the Ti/Ag target increases and the Ti fraction decreases as the Ag pellets are being placed on the Ti erosion track, this result is somewhat expected. In fact, by taking a closer look at Fig. 2b), it is possible to see that N/Ti stoichiometry gradually changes to close-stoichiometry almost throughout all coatings, with ratios very close to 0.8-1. For the highest Ag concentrations, however, a steep decrease of the N/Ti ratio is observable,

with values close to 0.3-0.5. In fact, Ti contents decrease steadily from 50 at.% to ~30 at.%, while N concentrations initially also decrease steadily from ~50 at.% to ~25 at.%, but then an abrupt decrease is observable, with values close to 11-15 at.%. This abrupt fall of N concentration causes the deposited films to change from stoichiometric to N-deficient Ag:TiN. Due to Ag low ISEE and high sputtering yield, as the Ag fraction in the target is continuously increased, the amount of species (mainly Ag) present in the reactor also increases, leading to a strong decrease of its mean free path. As no substrate bias voltage was used during the sputtering process, the available amount of nitrogen cannot easily react with the growing films due to mobility constraints [14].

3.3. Electrical and Thermal properties: analysis and discussion

As stated before, one of the main requirements to develop a coating system that may be suitable for biopotential electrode applications is its good conductivity. Fig. 3 shows the resistivity variation as a function of the Ag/(Ti+N) ratio. Once again, the three-zone behaviour is patent in the resistivity evolution. The samples prepared within zone I exhibit relatively high resistivity values (between ~2.25×10^{-5} to 3.25×10^{-5} Ω·m), which may, at first glance, seem not very typical for stoichiometric TiN films [46]. Anyway, it is important to focus is that the preparation conditions used were quite specific due to the targeted application – a thin film system to be used in bio-electrodes, namely those for electroencephalography, EEG, and electrocardiography, ECG. In fact, the base substrates for the bio-electrodes are being built from relatively simple and well-known polymers: polyurethane, polycarbonate and polyethylene. A major concern in these substrates is that the thin films deposition conditions must not be too severe in order to avoid their melting or some kind of consistency problems such as deformation, structural and/or morphological changes in the polymers. For this, the deposition temperature of the films was fixed in a rather low value (not exceeding 100 ºC), and the films were grown in grounded condition (no bias). Using these conditions, the adatom mobility was significantly reduced, which resulted in structural and morphological arrangements in the films that are certainly far from being optimized, as it will be

shown latter in the text. With this, one should expect relatively high values of resistivity, manly in the almost pure TiN films (zone I films), when compared to other TiN films prepared with high adatom mobility, such as in the films that were prepared in the group at higher temperatures (250 ºC) and using ion bombardment of several dozens of negative voltages [46].

Moreover, one can also consider that low Ag contents can also promote some increase of resistivity, which would be an indication that it could be acting as an impurity. For intermediate Ag concentrations in the coatings, resistivity decreases abruptly from ~2.25×10^{-5} to 5.2×10^{-7} Ω·m, denoting that Ag, acting as a high conductivity dopant [23], promotes the desired effect for the envisaged application. Moreover, zone III resistivity values are actually below that of the bulk Ti (~4.5×10^{-7} Ω·m [47]). For the highest Ag content (Ag/(Ti+N) > 0.4), a resistivity of ~1.4×10^{-7} Ω·m is attained.

To further investigate the electrical response of the films, the morphology of the deposited samples was studied by SEM. Fig. 4 a_{1-3}) depicts the cross-section images, while Fig. 4 b_{1-3}) shows the top view and Fig. 4 c_{1-3}) the backscattered micrographs of the Ag:TiN films, corresponding to zone I, II and III, respectively. Fig. 4 a_4 - b_4 displays cross-section and top view images for the pure Ag film. The zone I films' high resistivity can be ascribed not only to the non-metallic characteristic of the low Ag content TiN-like coatings, but also to the well-known pyramid top columns [5] which, in turn, exhibit some degree of porosity and roughness. Non-uniform, rough and porous surfaces are known to hinder charge carrier mobility, thus reducing the films' conductivity. The low deposition rate in these zone I films (Fig. 1) correlates with a low film thickness [48], fact that can also explain the high resistivity values. K.-Y. Chan et al. [48], after studying the thickness dependence on the electrical properties of Cu thin films, state that thicker coatings promote an enhanced microstructure (less defects) and crystalline quality which, in turn, lead to surface energy minimization and to a reduction in grain boundary scattering due to charge carriers. Once all films were grown for 1h, thickness values can be directly extracted from the deposition rate: zone I and zone II films can be considered low thickness coatings (from ~1.0 to ~1.3 μm), while zone III can

be indexed to high thickness films (from ~1.3 to ~1.8 μm). As for zone II coatings (Fig. 4 a_2-c_2) it is possible to see that the TiN matrix columns appear to become more disaggregated than in zone I coatings, although a strong decrease in resistivity was noticed. Moreover, a steep incorporation of high conductivity Ag occurs within this zone II, leading to the formation of Ag clusters/aggregates that extensively and uniformly cover the coating's surface. This result is consistent with the work of de los Arcos et al. [49] where the authors reported the formation of spherical Ag clusters embedded in the TiN matrix and also partially sitting on the surface. In fact, deep embedded clusters were also found in this work (Fig. 4 c_2). So, as the Ag incorporation increases within zone II, two phenomena occur: (i) the surface becomes more and more uniformly covered with the reported Ag clusters whereas (ii) the TiN matrix becomes increasingly embedded with smaller aggregates between its columns, that will eventually reach the percolation threshold, thus strongly changing the samples resistivity behaviour from non-metallic to metallic. The strong Ag incorporation and segregation that occur within zone II samples, in fact, seem to overcome the low-thickness regime that theoretically imposes higher resistivity values. When the highest Ag concentration and film thickness is reached – zone III coatings, Fig. 4 a_3-c_3) – the morphology of the films changes dramatically. The columnar features are lost and the coatings develop a more granular, compact and rough morphology, similar to pure Ag thin films [50] (Fig. 4 a_4 and b_4). This morphological evolution can be related to the fact already mentioned that the TiN matrix is gradually changing from stoichiometric to N-deficient as Ag concentration increases, which in turn also exhibits a granular-like compact structure [5]. The low resistivity of the samples from this zone can be in part ascribed to the combination of these morphological changes, as the content of high conductivity Ag is quite substantial and the sputtered films are very compact, dense and thick, which are prerequisites to low resistivity values. It is interesting to note that Ag clusters are still present in the coating's surface (Fig. 4 b_3), although smaller in size when compared to zone II ones, but no embedded aggregates are visible (Fig. 4 c_3). This could mean that some fraction of Ag may be dissolved in the N-deficient TiN matrix, opening the door to a possible formation of a TiAg

intermetallic.

In order to further understand the growth mechanisms and the influence of the observed features patent in SEM observations on the resistivity evolution, a comprehensive structural characterization of the Ag:TiN samples was performed. Fig. 5 shows the XRD diffractograms of the sputtered samples, taking into account their increasing Ag content. Once more, the three-zone behaviour is clearly visible, which is in great accordance with all previous analyses. A very close correlation between SEM observations and XRD data can be claimed, with the Ag distribution in the TiN matrix playing a pivotal role in the overall behaviour. Taking a closer look at Fig. 5 a), where the full range diffractograms are shown, zone I comprises, once more, only the stoichiometric TiN reference sample and the low Ag content one (0.1 at.%). Both coatings are highly textured, exhibiting a preferential fcc-TiN (111) growth (ICDD card no. 00-038-1420), typical for stoichiometric TiN films [5, 14, 46]. No Ag peaks were detected in the 0.1 at.% Ag sample due to the fact that the amount of incorporated Ag (as well as its grain size) may be too low to be detected [51]. The indistinguishable structural differences between these TiN-like coatings that comprise zone I may justify the rather similar high resistivity values, which remain close to that of TiN. As for zone II coatings, the preferential growth remains the same as the one for zone I films (fcc-TiN (111)), although some changes are clearly visible. A new peak at ~42.5º corresponding to the fcc-TiN (200) phase becomes perceivable from 20.2 at.% Ag contents onwards, while the fcc-TiN (222) peak shifts to lower diffraction angles for Ag contents ranging from 6.3 to 14.2 at.% and disappears almost completely from 20.2 at.% onwards. In fact, the main fcc-TiN (111) peak also shifts to lower 2θ angles and its intensity strongly decreases as well (Fig. 5 b). It indicates that the fcc-TiN structure is progressively destroyed by the formation of a new fcc-Ag (111) phase (ICDD card no. 00-004-0783), as a new peak rises at ~38º. The authors ascribe this peak to fcc-Ag (111), as several pure Ag aggregates are visible sitting on the surface and embedded in the TiN matrix of zone II coatings (Fig. 4). However, due to the fact that the tetragonal TiAg (111) peak (ICDD card no. 00-006-0560) occurs at approximately the same diffraction angle, the formation of a TiAg

intermetallic may not be excluded, although unlikely, once zone II TiN matrix is stoichiometric or close-stoichiometric, with almost all interstitial sites occupied by N atoms). In addition, the slight shift towards lower 2θ angles referred above, suggests the presence of small Ag inclusions in the fcc-TiN structure. Zone II is, in fact, a transition zone strongly defined by a steep decrease of the resistivity values (Fig. 3). It is now clear that a new highly conductive fcc-Ag phase, in the form of clusters, is produced sitting on the surface and embedded in an increasingly less crystalline TiN matrix. Gulbiński and Suszko [52] claimed that for high Ag contents, grain boundary segregation occurs, hindering the growth of the metallic nitride matrix and decreasing its crystallinity. Zone II and especially zone III data are in agreement with this claim, as for higher Ag concentrations the sputtered films exhibit a very low degree of crystallinity, with very broad peaks and baseline noise clearly patent, as it is possible to see from Fig. 5 b). To note that the fcc-TiN (111) peak of the highest Ag concentration sample (47.5 at.%) exhibits a strong shift towards high diffraction angles, corroborating the assumption that the TiN matrix formed may be N-deficient, offering the possibility of some Ag atoms occupying interstitial sites (potential formation of TiAg intermetallics), thus exhibiting lower lattice parameters. These results are, as stated before, in great consistence with SEM observations (Fig. 4), where it is possible to see a gradual increase of the compactness of the films, with the organized columnar growth being progressively lost as the Ag content increases and also with composition analysis (Fig. 2), confirming the formation of a N-deficient TiN matrix for high Ag contents. To summarize, the growth behaviour of the Ag:TiN films provides a coherent justification to the resistivity evolution. As Ag content increases, the fcc-TiN structure is continuously hindered while the formation of a new highly conductive fcc-Ag phase takes place (in fact, fcc-Ag (111) phase becomes the preferential one for the highest Ag contents). This means that, as stated above, the sputtered films are evolving from a compound/nitride-based to a metallic-like character, thus exhibiting an overall decrease of the resistivity values.

In analytical terms, the resistivity of thin films can be expressed by the well-known

Matthiessen's rule [48]:

$$\rho = \rho_p + \rho_m + \rho_f + \rho_i + \rho_s \quad (2)$$

where ρ_p, ρ_m, ρ_f, ρ_i and ρ_s represent the resistivity caused by scattering from phonons, impurities, defects, grain boundaries and the surface scattering, respectively. The scattering effect from impurities must not be considered, once no major impurities were detected in the composition analysis such as oxygen or argon inclusions. If present, their content should be within the standard error of the RBS technique, which is 3-4 at.%. Also, no important defects are perceivable in the coatings. Taking into account the Fuchs-Sondheimer (F-S) model [53, 54], the resistivity contribution due to the scattering effect of conduction electrons at the film's surface should also be disregarded, as the surface scattering effect only becomes relevant when the film's thickness is below the mean free path of the conduction electrons. All sputtered Ag:TiN coatings exhibit thicknesses > 1 μm, thus being well above the electron mean free path of Ti and Ag, both in the range of tens of nanometres. Consequently, only the scattering from phonons and grain boundaries contributions should be taken into account, once the chemical composition of the samples is an important variable (already analysed) and the role of grain size evolution should also be fundamental.

Consequently, the grain size evolution was investigated as function of the Ag/(Ti+N) ratio, taking into account the predominant fcc-TiN (111) and Ag (111) phases, as shown in Fig. 6. It is possible to see that the presence of small Ag incorporations – within zone I films – translates into a decrease of the grain size when comparing with the stoichiometric TiN reference coating. It must be remembered that no Ag (111) phase was detected in the 0.1 at.% Ag sample. Although no differences were detected in the XRD diffractograms, small additions of Ag have a profound effect on the grain size of the growing zone I films, decreasing from ~37 nm to ~22 nm. Once more, the rather high TiN-like resistivity values that are exhibited by low-Ag concentration samples are in great accordance with grain size data. It is known that grain size evolution is inversely connected to the resistivity [47], meaning that a decrease of the grain size is expected to give rise to an increase

of the resistivity. As for zone II films, the previous relation is also valid, once a substantial increase of grain size values (until ~75 nm and ~30 nm for TiN (111) and Ag (111) phases, respectively) for the first samples within zone – 6.3-14.2 at.% Ag – leads to a strong decrease of resistivity. This is also consistent with XRD data, since it is possible to see (Fig. 5 b) a slight increase of both fcc-TiN (111) and Ag (111) peaks' intensity and definition, indicating an improvement of the crystallinity of the films, thus leading to low resistivity values. However, above 20.2 at.% Ag, a progressive decrease of the crystalline size values of the coatings take place (as explained before), and although polycrystalline, the films seem to become less crystalline – zone III –, a fact that is proven by the accentuated decrease of grain size from ~75 nm to ~15 nm for fcc-TiN (111) phase and from ~30 nm to ~10 nm for fcc-Ag (111). Therefore, with such strong decrease of crystallinity, an increase of the resistivity values was expected. In fact, the opposite is observed since the resistivity values further decrease in zone III. This could mean that the main contribution to resistivity is not related to grain boundary scattering, but scattering from phonons instead (due to the strong composition changes evidenced throughout the range of sputtered Ag:TiN films), confirming the paramount importance of Ag incorporation as the main controlling mechanism of the exhibited behaviour throughout all characterization performed.

In fact, Ag may also be significantly increasing the charge carrier density, thus probably depleting the grain boundary scattering effect. Furthermore, Kitawaki et al. [55] suggested that Ag solidifies in the faces of the fcc-TiN cube, fact that may promote the formation of some kind of electronic path between the TiN grains, thus strongly decreasing the samples' resistivity. It is important to note that zone II and zone III samples exhibit strong Ag segregation (see Fig. 4) at the surface and in between the TiN columns, corroborating this assumption. Kitawaki et al. mechanism of Ag:TiN formation [55] is, indeed, in complete accordance with what is observed in the current study, considering a perfect TiN nanocrystalline structure (no N vacancies), which is true for zone I and zone II coatings (see Fig. 5). As for zone III, the high amounts of Ag may in some way encapsulate the fcc-TiN cubes (and even form Ti-Ag metal-metal bonding, once TiN is N-

deficient), hindering their growth into columnar features (as suggested above), therefore leading to a more compact metallic-like structure.

As claimed before, all evidences show that the coatings are steadily changing from a nitride/compound-like (zone I) to a metallic-like (zone III) behaviour with a transition zone (zone II) in between. The resistivity evolution follows coherently this change, decreasing roughly two orders of magnitude from the lowest to the highest silver additions. Moreover, a recent study of the group showed that not only the resistivity is showing promising behaviour taking into account the targeted application, but also the Young's modulus is showing an important variation regarding common TiN known values. In fact, not only the values of the Young's modulus seem to decrease in about 10% as the silver amounts increase (from ~200 GPa to ~180 GPa, by varying Ag from ~20 to ~36 at.%), but they also reduce significantly with the annealing temperature, corresponding to structural and morphological changes that are induced [56]. This change can also be claimed from the observation of the thermal characteristics. The results presented are interpreted assuming a two-layer system, being the first layer the Ag:TiN film and the second layer the substrate. No interfacial thermal resistance was considered. In order to ensure that all the information related to the electronic path of the signal is suppressed, the Modulated IR Radiometry signals were normalized, using a semi-infinite opaque body of smooth surface. The resulting normalized amplitude and phase lag signals can directly be compared with the theoretical solutions for a two-layer system [57]. According to the two-layer method [57], the modulation frequency and the respective phase lag are measured at the relative extrema of the inverse calibrated frequency-dependent phase lag signals, in the range of the intermediate modulation frequencies. The obtained measurements contain direct information on the sample's thermal diffusion time and about the ratio of the thermal effusivities of the two layers (e_c/e_b). The subscript c refers to coating and b to the substrate. The determination of the thermal effusivity of the sample (once e_b is usually know from literature) allows one to get the thermal conductivity (k), according to the following simple relations, where ρ represents the density and c the specific heat:

$$e = \sqrt{(k\rho c)} = k/\sqrt{\alpha} \rightarrow k = e\sqrt{\alpha} \quad (3)$$

Fig. 7 shows the evolution of the ratio of the thermal effusivities of the two layers, as a function of the Ag/(Ti+N) ratio, for a set of Ag:TiN samples. Following a quite similar change tendency, the results obtained indicate that there are clearly two major zones of samples, with very similar limits as those reported before for the electrical characterization as well as for the morphological and structural evolutions. The first major zone (corresponding to the previously identified zone I) reveals relatively high values of the effusivity ratio, while the second (previously identified zone III) has the lowest set of values for this same ratio. Zone II acts, again, as a transition zone. Furthermore, and in spite of the well-known different mechanisms that rule electrical and thermal conduction behaviours, it is also worth noticing that the type of values obtained in these two zones (almost constant and relatively high in the first and relatively low in the second) have a noticeable similarity to what was observed for the electrical variation, Fig. 3. In this way, it seems reasonable to claim that, again, the changes in the film's composition and the subsequent changes in both morphological and structural features are the most probable parameters that may explain such thermal behaviour. The changes in the crystalline growth that are clear within the films from both zones I and III, associated with the clear decrease of the crystalline sizes of the films from zone III (Fig. 3 and Fig. 5 results) are probably inducing a decrease of phonon transport through the thin film, thus reducing the film effusivity. Nevertheless, it is important to discuss two possible mechanisms that may act in opposite ways. First of all, there is the grain size reduction and the tendency for a decrease in the thermal transport properties, but one must also bring up the fact that silver phases are being formed in zone II and III films, as previously discussed. If a pure Ag phase is being grown in these zones (as it seems to be probable), one would expect that an increase of the film effusivity should occur, given the well-known good thermal conduction properties of this element. The fact that the opposite was in fact observed (a decrease of film's effusivity), the conclusion is that the very weak crystalline phases that are formed are actually the most important factor for the effusivity evolution. Anyway, it should also be noted that a possible weak thermal

behaviour of a Ti-Ag phase that may be formed could account also for a decrease of the effusivity as it was observed.

4. CONCLUSIONS

In this work, nanocomposite Ag:TiN coatings were successfully sputtered in a wide range of compositions, ranging from 0 to ~50 at.% Ag and characterized, aiming at selecting the best compositional region for the use as biopotential electrodes. Throughout all characterization performed, the behaviour of the whole set of produced coatings can consistently be ascribed to three major zones. It was found that the main governing mechanism affecting the behavioural indexing of the films into the three zones was Ag incorporation in the TiN matrix. Consequently, the coatings in zone I ($0 \leq$ Ag at.% < 4.3), despite their high degree of crystallinity (only fcc-TiN phases were detected), exhibit rather high TiN-like resistivity values due to its porous/disaggregated pyramid-like columnar structure, that also lead to high effusivity ratios. This zone I comprehend the samples whose behaviour can be considered as nitride/compound-like. As for zone II ($4.3 \leq$ Ag at.% < 33.2) coatings, the resistivity values suffer a strong decrease due to the formation of highly conductive Ag phases (aggregates) sitting on top and also embedded in the TiN matrix (hindering its growth), reaching the percolation threshold. The effusivity ratios also suffer a steep decrease due the strong reduction of the coatings' crystallinity, thus reducing the phonon transport phenomenon. Zone II can hence be considered as a transition zone, as it leads to a completely metallic-like behavioural zone – zone III ($33.2 \leq$ Ag at.% ≤ 47.5). The polycrystalline and compact Ag:TiN thin films ascribed to this zone III exhibit the lowest resistivity (even below bulk Ti) – although not very different from the samples with the most Ag content within zone II – and effusivity ratios, due to large incorporation/formation of highly conductive Ag phases. It is also important to refer that for the highest Ag contents the TiN matrix becomes N-deficient, opening the possibility for the formation of a Ti-Ag intermetallic.

Taking into account the envisaged application, and bearing in mind that low resistivity materials are preferable to be used as biopotential electrodes, the coatings from the top-end of zone II and the films from zone III (with Ag contents ranging from ~20 to ~50 at.%) seem to be, a priori, the most suitable ones.

ACKNOWLEDGEMENTS

This research is partially sponsored by FEDER funds through the program COMPETE – Programa Operacional Factores de Competitividade and by national funds through FCT – Fundação para a Ciência e a Tecnologia, under the projects PEst-C/EME/UI0285/2011, PTDC/SAU-ENB/116850/2010, PTDC/CTM-NAN/112574/2009 and Programa Pessoa 2012/2013 Cooperação Portugal/França, Project nº 27306UA Porous architectures in GRAded CERamic thin films for biosensors - GRACER. The authors would also like to acknowledge CEMUP for SEM analysis. P. Pedrosa acknowledges FCT for the Ph.D. grant SFRH/BD/70035/2010.

BIBLIOGRAPHY

1. M. Teplan**,** Meas. Sci. Rev., 2 (2) (2002) 1-11.
2. E. McAdams, " Bioelectrodes ", in Encyclopaedia of Medical Devices and Instrumentation, Webster J. G. Ed., New York, Wiley, (1988) 120-166.
3. A. Searle, L. Kirkup, Physiolog. Meas. 22 (2000) 271-283.
4. W.K. Ko, J. Hynecek, "Dry electrodes and electrode amplifiers", in H.A. Miller and D.C. Harrison (Eds), Biomedical Electrode Technology, Academic Press, New York (1974).
5. L.T. Cunha, P. Pedrosa, C.J. Tavares, E. Alves, F. Vaz, C. Fonseca, Electrochim. Acta, 55 (1) (2009) 59-67.
6. G. Gargiulo, R.A. Calvo, P. Bifulco, M. Cesarelli, C. Jin, A. Mohamed, A. van Schaik, Clin. Neurophysiol. 121 (5) (2010) 686-693.
7. C. Fonseca, J.P. Silva Cunha, R.E. Martins, V. Ferreira, J.P. Marques de Sá, M.A. Barbosa, A. Martins Silva, IEEE Trans. Biomed. Eng. 54 (1) (2007) 162-165.
8. K.-P. Hoffmann and R. Ruff, Proceedings of the 29th Annual International Conference of the IEEE EMBS, Lyon, France, August, (2007) 23-26.
9. J. Baek, J. An, J. Choi, K. Park, S. Lee, Sens. Actuators, A 143 (2008) 423–429.
10. A. Gruetzmann, S. Hansen, J. Muller, Physiol. Meas. 28 (2007) 1375–1390.
11. V. Marozas, A. Petrenas, S. Daukantas, A Lukosevicius, Journal of Electrocardiology 44 (2011) 189–194.
12. S. Piscanec, L. Ciacchi, E. Vesselli, G. Comelli, O. Sbaizero, S. Meriani, A. De Vita, Acta Mater. 52 (2004) 1237.
13. P. Pedrosa, E. Alves, N.P. Barradas, P. Fiedler, J. Haueisen, F. Vaz, C. Fonseca, Corros. Sci. 56 (2012) 49–57.
14. S.L. Chui, J. Leu, P.S. Ho, J. Appl. Phys. 76 (1994) 5136.
15. O. Kraft, M. Hommel, E. Arzt, Mater. Sci. Eng., A 288 (2000) 209.
16. M. Hommel, O. Kraft, Acta Mater. 49 3935 2001.
17. B.E. Alaca, M.T.A. Saif, H. Sehitoglu, Acta Mater. 50 (2002) 1197.
18. D.Y.W. Yu, F. Spaepen, J. Appl. Phys. 95 (2003) 2991.
19. S.P. Lacour, S. Wagner, Z. Huang, Z. Suo, Appl. Phys. Lett. 82 (2003) 2404.
20. Y. Xiang, T. Li, Z. Suo, J. Vlassak, Appl. Phys. Lett. 87 (2005) 161910.
21. R.M. Niu, G. Liu, C. Wang, G. Zhang, X.D. Ding, J. Sun, Appl. Phys. Lett. 90 (2007) 161907.
22. R.X. Wang, X.M. Tao, Y. Wang, G.F. Wang, S.M. Shang, Surf. Coat. Technol. 204 (2010) 1206–1210.

23. R.C. Adochite, D. Munteanu, M. Torrell, L. Cunha, E. Alves, N.P. Barradas, A. Cavaleiro, J.P. Riviere, E. Le Bourhis, D. Eyidi, F. Vaz, Appl. Surf. Sci. 258 (2012) 4028–4034.
24. H. Chiriac, M. Urse, F. Rusu, C Hison, M. Neagu, Sens. Actuators, A 76 (1999) 376-380.
25. K.-H. Liao, K.-L. Ou, H.-C. Cheng, C.-T. Lin, P.-W. Peng, Appl. Surf. Sci. 256 (2010) 3642-3646.
26. M. Fiori, M. Paula, A. Bernardin, H. Riella, E. Angioletto, Mater. Sci. Eng., C 29 (2009) 1569–1573.
27. M. Santos, C. Oliveira, C. Tachinski, M. Fernandes, C. Pich, E. Angioletto, H.G. Riella, M. Fiori, Int. J. Miner. Process. 100 (2011) 51–53.
28. P.J. Kelly, H. Li, K.A. Whitehead, J. Verran, R.D. Arnell, I. Iordanova, Surf. Coat. Technol. 204 (2009) 1137–1140.
29. P.J. Kelly, H. Li, P.S. Benson, K.A. Whitehead, J. Verran, R.D. Arnell, I. Iordanova, Surf. Coat. Technol. 205 (2010) 1606–1610.
30. L.A. Geddes, L.E. Baker, A.G. Moore, Med. Biol. Eng. 7 (1969) 49-56.
31. N.P. Barradas, C. Jeynes, R.P. Webb, Appl. Phys. Lett. 71 (1997) 291.
32. A.F. Gurbich, Nucl. Instr. and Meth. B, 268 (2010) 1703.
33. L.J. van der Pauw, Philips Res. Repts. 13 (1958) 1-9.
34. F. Macedo, F. Vaz, M. Torrell, R.T. Faria Jr., A. Cavaleiro, N.P. Barradas, E. Alves, K.H. Junge, B.K. Bein, J. Phys. D: Appl. Phys. 45 (2012) 105301.
35. D. Depla, S. Heirwegh, S. Mahieu, J. Haemers, R. De Gryse, J. Appl. Phys. 101 (2007) 013301.
36. D. Depla, G. Buyle, J. Haemers, R. De Gryse, Surf. Coat. Technol. 200 (2006) 4329– 4338.
37. D. Depla, S. Mahieu, R. De Gryse, Thin Solid Films 517 (2009) 2825–2839.
38. J.A. Thornton, J. Vac. Sci. Technol. 15 (1978) 171.
39. J.M. Chappé, F. Vaz, L. Cunha, C. Moura, M.C. Marco de Lucas, L. Imhoff, S. Bourgeois, J.F. Pierson, Surf. Coat. Technol. 203 (2008) 804-807.
40. J. Borges, F. Vaz, L. Marques, Appl. Surf. Sci. 257 (2010) 1478–1483.
41. J. Borges, N. Martin, N.P. Barradas, E. Alves, D. Eyidi, M.F. Beaufort, J.P. Riviere, F. Vaz, L. Marques, Thin Solid Films 520 (2012) 6709–6717.
42. R. Arvinte, J. Borges, R.E. Sousa, D. Munteanu, N.P. Barradas, E. Alves, F. Vaz, L. Marques, Appl. Surf. Sci. 257 (2011) 9120– 9124.
43. J.F. Pierson, D. Wiederkehr, A. Billard, Thin Solid Films 478 (2005) 196–205.
44. V. S. Smentkowski, Prog. Surf. Sci. 64 (2000) 1-58.

45. C.D. Wanger, W.M. Riggs, L.E. Davis, J.F. Moulder, G.E. Muilenberg, Handbook of X-ray Photoelectron Spectroscopy, Perkin-Elmer Corp., Physical Electronics Division, Eden Prairie, Minnesota, USA, 1979.
46. F. Vaz, J. Ferreira, E. Ribeiro, L. Rebouta, S. Lanceros-Méndez, J.A. Mendes, E. Alves, Ph. Goudeau, J.P. Rivière, F. Ribeiro, I. Moutinho, K. Pischow, J. de Rijk, Surf. Coat. Technol. 191 (2005) 317–323.
47. M.E. Day, M. Delfino, J.A. Fair, W. Tsai, Thin Solid Films 254 (1995) 285-290.
48. K.-Y. Chan, T.-Y. Tou, B.-S. Teo, Microelectron. J. 37 (2006) 608-612.
49. T. de los Arcos, P. Oelhafen, U. Aebi, A. Hefti, M. Düggelin, D. Mathys, R. Guggenheim, Vacuum 67 (2002) 463–470.
50. Y. Xiong, H. Wu, Y. Guo, Y. Sun, D. Yang, D. Da, Thin Solid Films 375 (2000) 300-303.
51. J.G. Han, H.S. Myung, H.M. Lee, L.R. Shaginyan, Surf. Coat. Technol. 163-164 (2003) 591-596.
52. W. Gulbiński, T. Suszko, Surf. Coat. Technol. 201 (2006) 1469–1476.
53. K. Fuchs, Proc. Camb. Philos. Soc. 34 (1938) 100.
54. E.H. Sondheimer, Phys. Rev. 80 (1950) 401.
55. Ko. Kitawaki, K. Kaneko, K. Inoke, J.C. Hernandez-Garrido, P.A. Midgley, H. Okuyama, M. Uda, Y. Sakka, Micron. 40 (2009) 308-312.
56. P. Pedrosa, D. Machado, M. Evaristo, A. Cavaleiro, C. Fonseca, F. Vaz, Vacuum (2013). Submited.
57. J.L. Nzodoum Fotsing, J. Gibkes, J. Pelzl, B.K. Bein, J. Appl. Phys. 98 (2005) 063522.

Table captions

Table I. Experimental parameters used in all depositions.

Deposition parameters	
Ar (Pa)	3×10^{-1}
N_2 (Pa)	3.4×10^{-2}
t (s)	3600
I ($A.cm^{-2}$)	$1x10^{-2}$
T (ºC)	100
Bias (V)	GND
P_{work} (Pa)	$3.5\text{-}3.8\times10^{-1}$
P_{base} (Pa)	$\sim10^{-4}$

Figure captions

Fig. 1. Evolution of the deposition rate and target potential with increasing Ag exposed area in the target.

Fig. 2. Evolution of the coatings' Ag content and Ag/(Ti+N) ratio as a function of the Ag exposed area in the target (a) and Ti-N-Ag composition ternary phase diagram (b).

Fig. 3. Coatings' resistivity evolution with increasing Ag content and Ag/(Ti+N) ratio.

Fig. 4. SEM cross-section (a_{1-4}), top (b_{1-4}) and backscattered (c_{1-3}) micrographs of the Ag:TiN (Zone I, II and III) and pure Ag coatings.

Fig. 5. XRD diffractograms as a function of Ag incorporation in the coatings; (a) full scale diffractograms and (b) 34-40º magnification.

Fig. 6. Grain size evolution with increasing Ag/(Ti+N) ratio.

Fig. 7. Two-layer thermal effusivity evolution as a function of the Ag/(Ti+N) ratio.

Figure 1

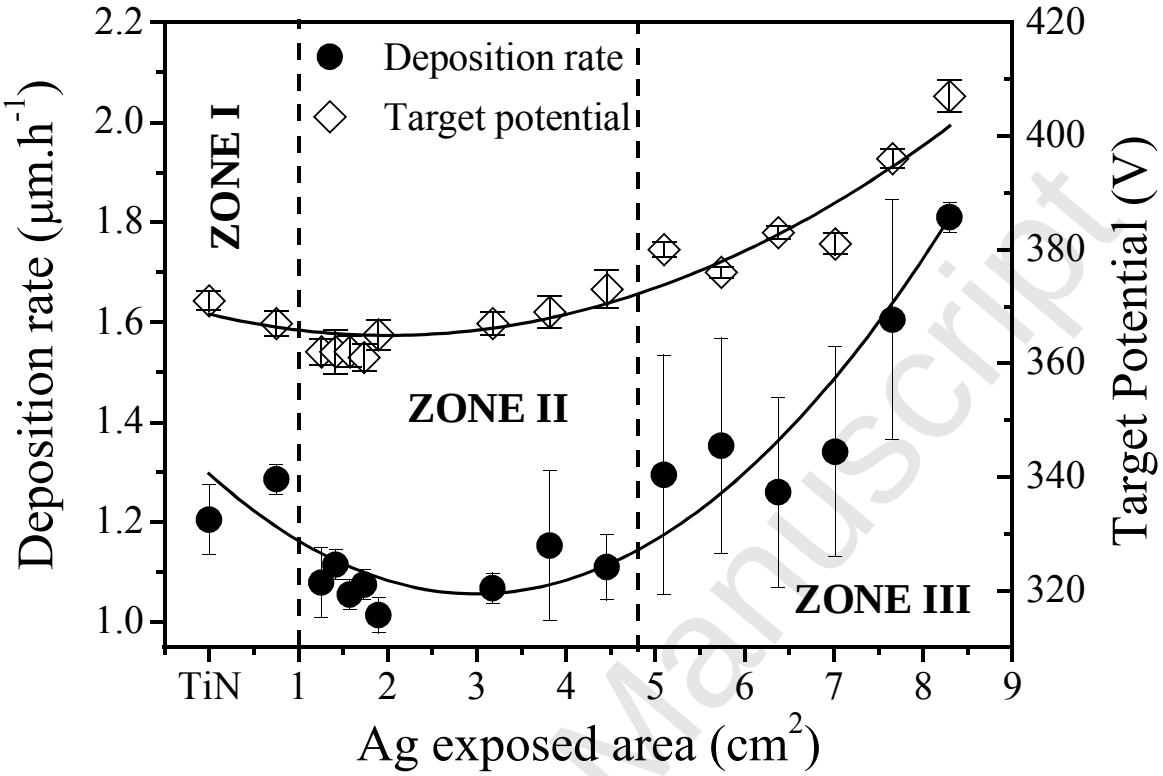

Figure 2

a)

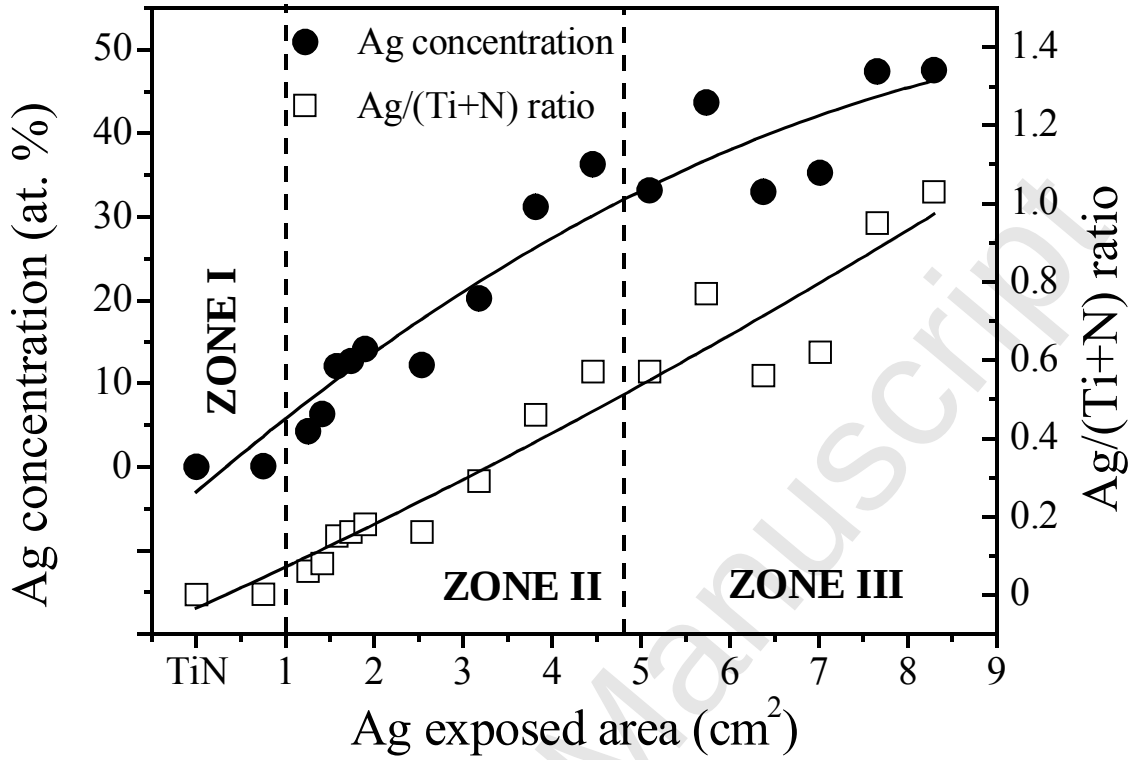

b)

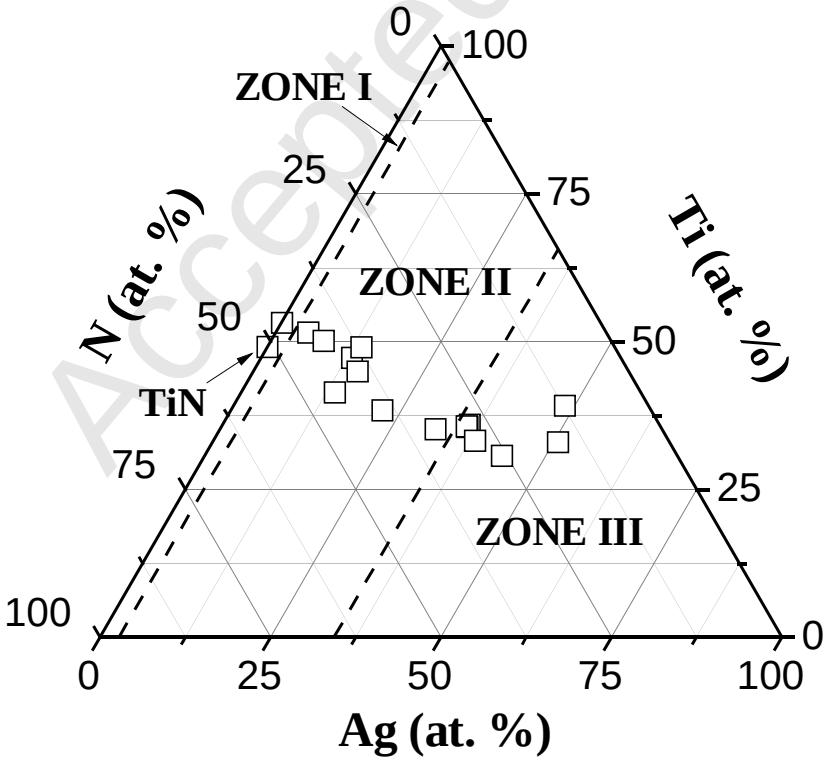

Figure 3

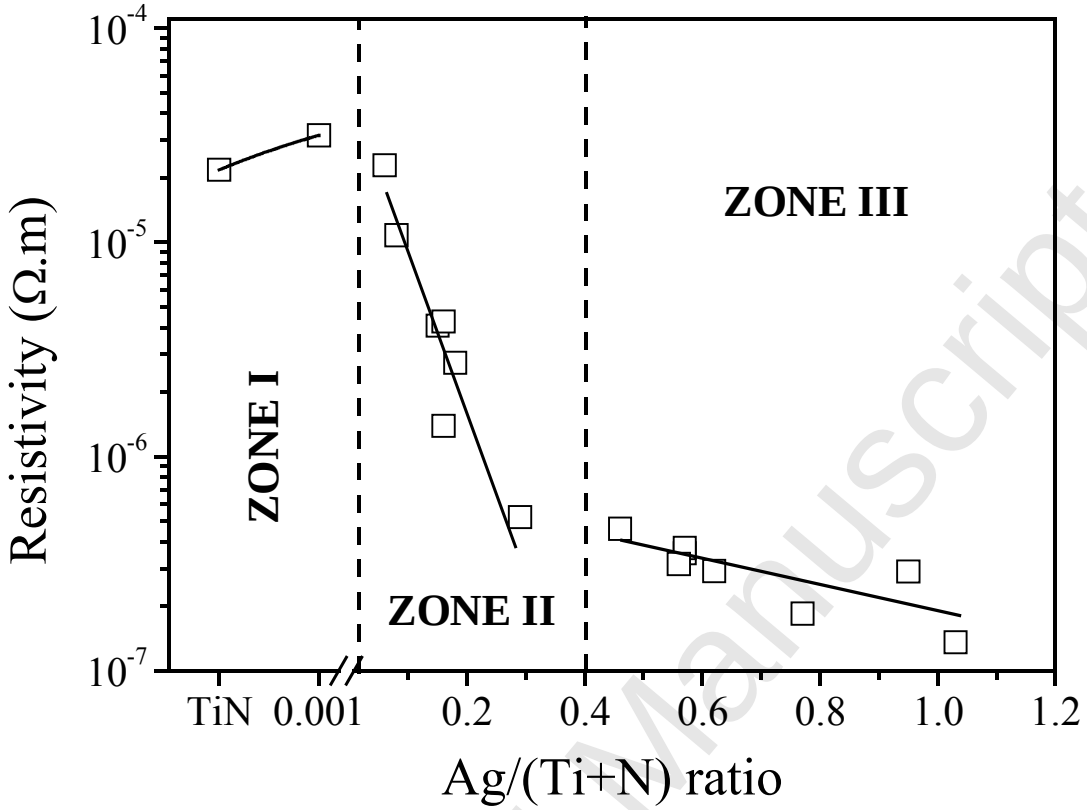

Figure 4

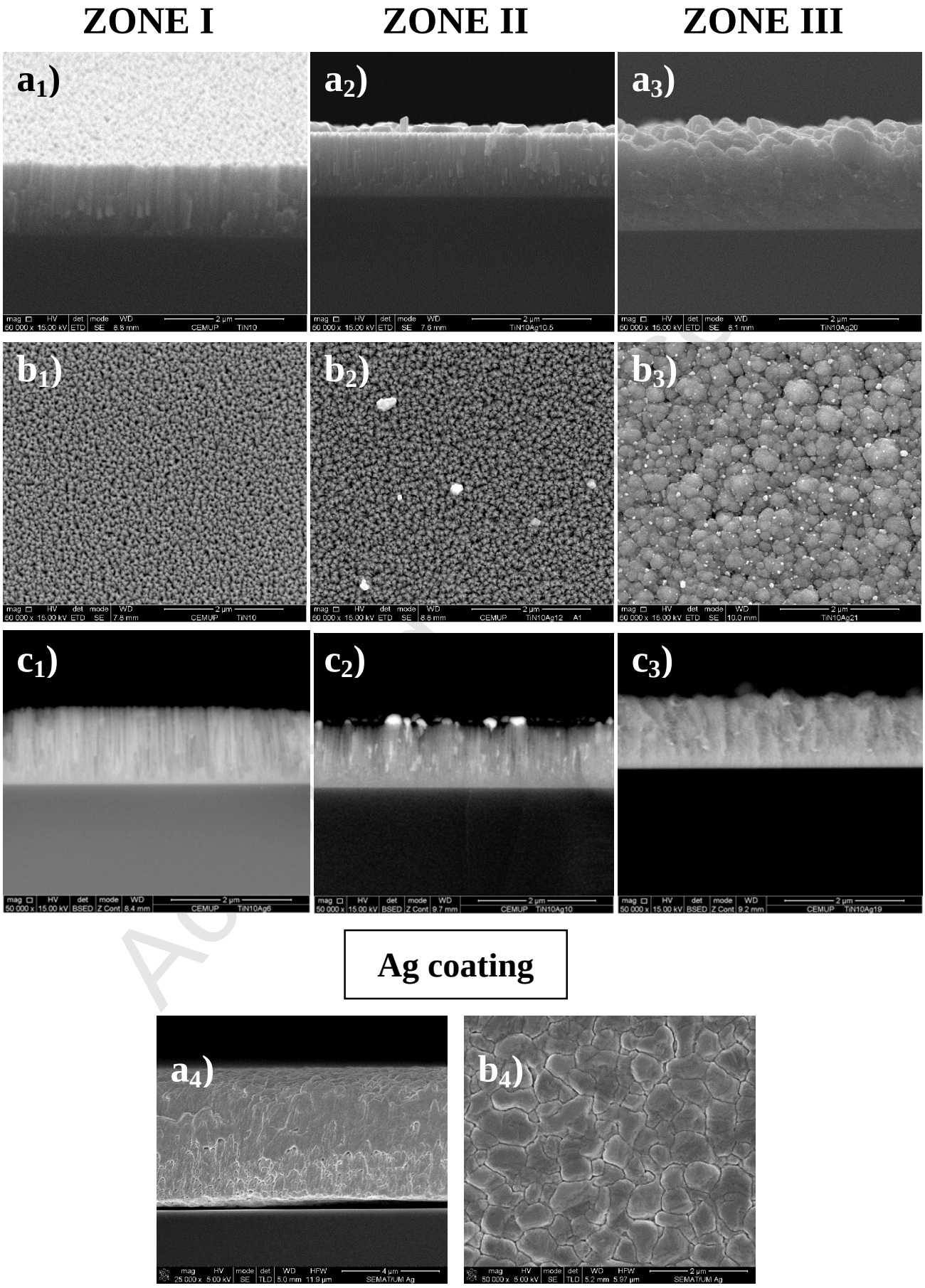

Figure 5

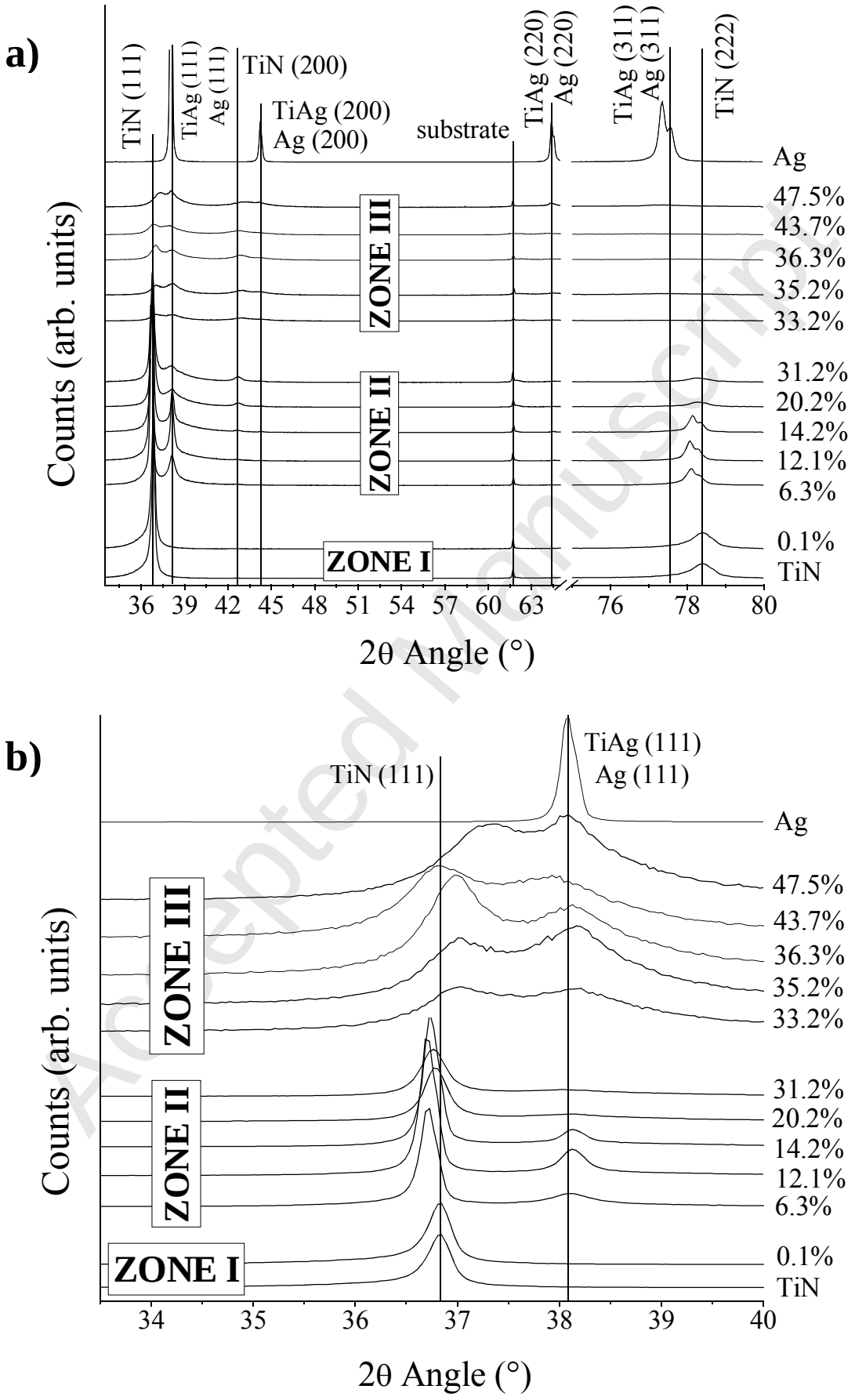

Figure 6

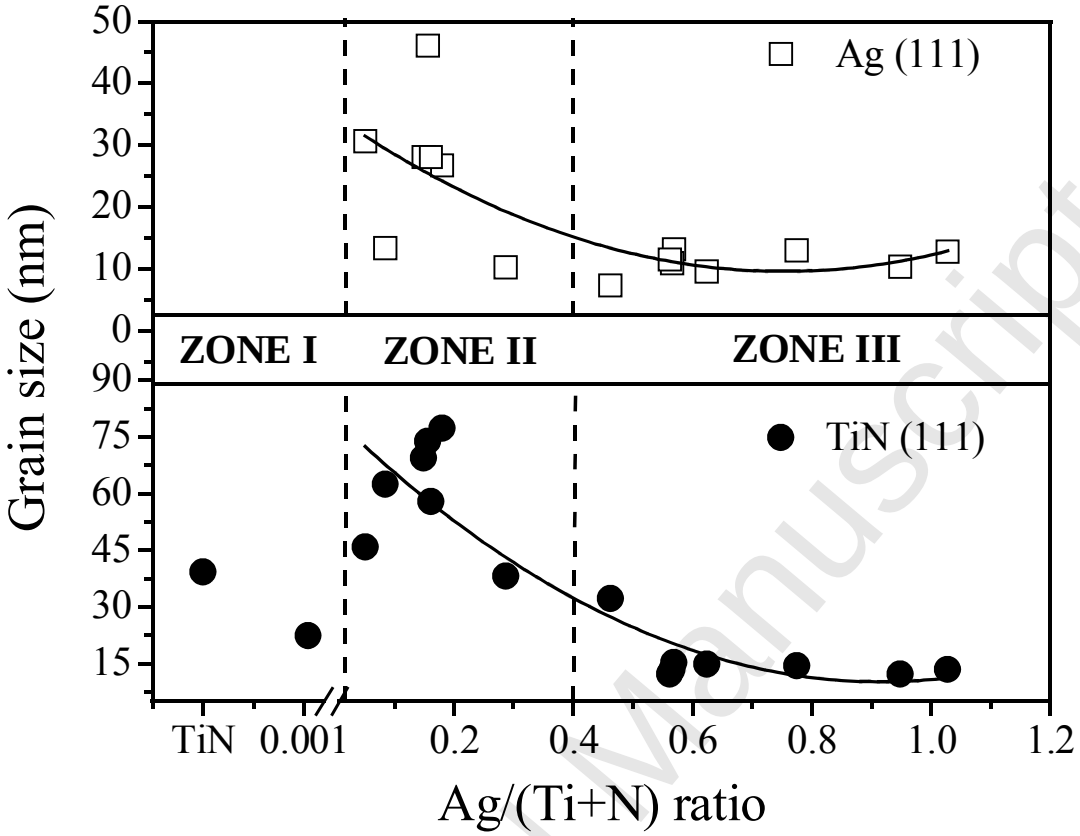

Figure 7